Development and Validation of a Robust Actuator Motion Controller for Real-time Hybrid Simulation

Xiuyu Gao, Nestor Castaneda and Shirley J. Dyke

{xygao, ncastan, sdyke} @ purdue.edu

Report IISL — 001, December 2011

Intelligent Infrastructure Systems Laboratory

Abstract

Real time hybrid simulation (RTHS) has increasingly been recognized as a powerful testing methodology to evaluate structural components and systems under realistic operating conditions. RTHS is a cost effective approach compared with large scale shake table testing. Furthermore it can maximally preserve rate dependency and nonlinear characteristics of physically tested (non) structural components. Although conceptually very attractive, challenges do exist that require comprehensive validation before RTHS should be employed to assess complicated physical phenomena. One of the most important issues that governs the stability and accuracy of a RTHS is the ability to achieve synchronization of boundary conditions between the computational and physical elements. The objective of this study is to propose and validate an H∞ design for actuator motion control in RTHS. Controller performance is evaluated in the laboratory using a worst-case substructure proportioning scheme. A modular, one-bay, one-story steel moment resisting frame (MRF) specimen is tested experimentally. Its deformation is kept within linear range for ready comparison with the reference analytical solution. Both system analysis and experimental results show that the proposed H_∞ controller can significantly improve both the stability limit and test accuracy compared to several existing strategies. Another key feature of the proposed controller is its robust performance in terms of unmodeled dynamics and uncertainties, which inevitably exist in all physical systems. This characteristic is essential to enhance test quality for specimens with nonlinear dynamic behavior, thus ensuring the validity of proposed approach for more complex RTHS implementations.

Acknowledgement: This work was supported in part by the U.S. National Science Foundation under Grant CNS-1028668 (MRI), CMMI-1011534 (NEESR), and by the Purdue University Cyber-Center Special Incentive Research Grant and the School of Mechanical Engineering at Purdue University.

Data presented herein will be available for download in the NEEShub (nees.org).

TABLE OF CONTENTS

CHAPTER 1
INTRODUCTION

The concept of pseudo-dynamic (PsD) testing and hybrid simulation has evolved for decades with implementations and applications considered worldwide [(Nakashima, 1999),(Blakeborough, 2001), (Magonette, 2001), (Wu, 2007)]. In this approach a physical portion of the structural system (e.g., a bridge column) is tested at very slow speeds, perhaps taking 100-1000 times longer than in real-time. At such a time scale, components of the structure that are well understood may be replaced with a computational model, yielding a hybrid test with computational and physical components.

The recent Vision 2020 report [NEES2010] developed by the earthquake engineering community emphasized the important goal of developing resilient communities through the pursuit of research topics that were previously not possible. Some of the most crucial questions from the Vision 2020 report [NEES2010] include: *1) How can we best implement new materials and components? 2) How should damage be modeled? 3) What is the impact of uncertainty in the design of civil infrastructure?* The desire to answer these important questions justifies the need for new simulation and hybrid simulation capabilities in the next generation of earthquake engineering research.

The new availability of effective hybrid testing capabilities will enable researchers perform more efficient and cost effective tests. Furthermore, more thorough investigations will be possible through the ability to reconfigure a test as an infinite number of other possible structures.

Real-time hybrid simulation (RTHS) offers the capability to preserve rate dependence when examining the behavior of any physical components. One of the main challenges in accurately reproducing local boundary conditions on the physical component when using RTHS is in dealing with the dynamics of the hydraulic actuator, including its interaction with the physical component. The potential detrimental effect of actuator dynamics in terms of test stability was interpreted as introducing negative damping (Horiuchi, 1999) into the RTHS system. A delay model was thus assumed and time domain prediction approach was proposed to reduce this delay. This concept was later generalized to consider time varying delay and an online estimation and compensation strategy was proposed (Darby, 2002). First order dynamic models have been assumed by other researches both in continuous (Lim, 2007) and discrete domain (Chen, 2010) and adaptive control laws were applied as an approach to deal with physical nonlinearities. Higher order models have been demonstrated to be more effective in capturing actuator dynamics over a broader frequency range (Carrion, 2007). Various feed-forward type of strategies have also been developed [(Shing, 2004), (Reinhorn, 2004), (Phillips, 2011)] that have mainly fallen into the scope of classical control design category. Nonlinear models for individual electro-hydraulic actuation components have been addressed (Merritt, 1967), based on which advanced nonlinear adaptive and robust control strategy was proposed (Yao, 2001) for high precision actuator motion control.

Although the ultimate goal in RTHS is to test unknown substructures, few past studies have thoroughly validated these methods using known reference solutions. Herein we propose and validate RTHS through comparison with an updated numerical model. A highly reconfigurable steel moment resisting frame (MRF) specimen is designed and erected in the Intelligent Infrastructure Systems Laboratory (IISL) at Purdue University as one of the first attempts to perform comprehensive validation of RTHS on a realistic structural specimen. Few publications have also addressed the importance of experimental design and its significant implication in RTHS implementation, when subjected to de-synchronization of the numerical and experimental states. A generalized approach is demonstrated herein to look into these issues from a dynamic system perspective. It is noted interestingly that the same amount of tracking error can have significant different influences on RTHS system stability and experimental error, depending on the composition of the computational and physical substructures. Given a specific experimental design, the proposed approach also establishes a quick way to estimate the maximum tolerable tracking error that will induce system instability. Off-line controller tracking performance assessment can therefore be linked to evaluate the risks prior to conducting an online RTHS.

An H_∞ controller is proposed for controlling the motion of servo-hydraulic actuators so that dynamically synchronized displacement boundary conditions can be achieved on the specimen interface nodes. The controller takes a unity-gain, negative-feedback form and the design is a trade-off between high open-loop gain of improved tracking performance and low gain of increased robustness. Robust stability becomes a major concern in a feedback control system when large system uncertainties and/or identification error occur. A low-pass filter is integrated into the original H_∞ controller formulation to accommodate relative large feedback measurement noise. When designed properly, the filter on the feedback path can be beneficial to further reduce phase lag and enhance the actuator tracking performance.

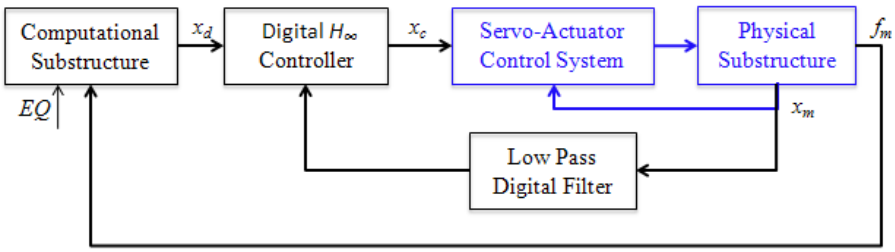

Figure 1: Proposed RTHS Implementation

The proposed RTHS main components are, a computational substructure; an outer-loop digital H_∞ motion tracking controller; an experimental component that includes both physical substructure and inner-loop analog servo-actuator control system; and potentially a correction mechanism that is used to consider the actuator-structure coupling and interaction to further improve the test accuracy. The dynamics of each component and their interactions through multiple feedback paths are schematically shown in *Figure **1***. Individual components are discussed in the following chapters and the

performance of the overall RTHS system is compared with reference structure system both analytically and experimentally.

Herein a worst-case scenario is proposed based on system analysis when the mass is primarily assumed in numerical substructure, while the stiffness of the structure is largely physically tested. This most imbalanced proportioning scheme introduces the largest artificial negative damping into the RTHS system. High precision actuator motion controller is thus essential since a fraction of a millisecond systematic tracking delay can induce test instability. A test matrix is constructed by varying numerical mass so that the overall RTHS system can respond at arbitrary resonance frequency. Several control strategies are evaluated for each specific experimental design. The experimental results show that the proposed H_∞ controller can nearly triple RTHS stability limit while still maintains smallest experimental error in general. Another test matrix is constructed to evaluate controller robustness by varying the P gain setting of servo-hydraulic controller. The proposed H_∞ controller appears to have advantages compared with other feed-forward control design strategies. It is observed that a small tracking error can induce a tremendously magnified RTHS error using the proposed validation test matrix. This problem is therefore ideal to evaluate actuator tracking control algorithm effectiveness in the context of RTHS implementation.

CHAPTER 2
PROBLEM FORMULATION AND MOTIVATION

Consider the case of a single-degree-of-freedom (SDOF) structure being divided into a numerical (denoted by subscript *n*) and an experimental (subscript *e*) portion. A certain amount of mass (*M*), stiffness (*K*) and damping (*C*) are assumed in each portion and the total reference structure system is the summation of both.

$$(M_n+M_e)\ddot{x}+(C_n+C_e)\dot{x}+(K_n+K_e)x=-(M_n+M_e)\ddot{x}_g \qquad \text{Equation 1}$$

Because perfect synchronization cannot be achieved in general, a RTHS implementation can be expressed using different state variables for each portion. Here x is defined as the displacement coordinate for the numerical model, and x_m as the experimentally measured displacement. The resulting equation is given as

$$M_n\ddot{x}+C_n\dot{x}+K_nx+M_e\ddot{x}_m+C_e\dot{x}_m+K_ex_m=-(M_n+M_e)\ddot{x}_g \qquad \text{Equation 2}$$

Without loss of generality it can be assumed that $x=A\sin\omega t, x_m=\Delta A\sin\omega(t-\delta t)$ where Δ and δt represent the amplitude and phase errors, respectively. By assuming a small δt**,** the de-synchronized states can be approximated through a Taylor series expansion as

$$\begin{aligned} x_m &= \Delta A\sin\omega(t-\delta t)\approx\Delta A(\sin\omega t-\omega\delta t\cos\omega t)=\Delta(x-\delta t\dot{x}) \\ \dot{x}_m &\approx \Delta(\dot{x}-\delta t\ddot{x}) \\ \ddot{x}_m &\approx \Delta(\ddot{x}+\omega^2\delta t\dot{x}) \end{aligned} \qquad \text{Equation 3}$$

A linearized RTHS system is therefore constructed by substituting Equation **3** into Equation **2**

$$(M_n+\Delta M_e-\Delta\delta tC_e)\ddot{x}+[C_n+\Delta C_e+\Delta\delta t(M_e\omega^2-K_e)]\dot{x}+(K_n+\Delta K_e)x=-(M_n+M_e)\ddot{x}_g \qquad \text{Equation 4}$$

A physical actuation control system normally introduces phase lag i.e. $\delta t>0$ so that the negative stiffness term K_e in Equation **4** plays the most critical role in RTHS stability. This observation is consistent with the conclusion obtained through an energy approach (Horiuchi, 1999). Another interesting observation is that the amount of mass reduction in Equation **4** is proportional to C_e which leads to a faster responded RTHS system when subjected to tracking delay.

The states in Equation **1** and Equation **4** are now synchronized so that a direct comparison can be made to gain additional insights into the behavior of the hybrid system.

Note that both Δ and δt can be very complicated and nonlinear in nature for a realistic physical system, especially when advanced control strategies are applied in a closed-loop system. Some cases are identified and discussed qualitatively below:

Case 1: Perfect synchronization is achieved with both $\Delta=1$ and $\delta t=0$. The RTHS system in Equation **4** is obviously identical to Equation **1**, reaching the ultimate goal of improving control performance and reducing RTHS error.

Case 2: When $M_n >> M_e, C_n >> C_e, K_n >> K_e$, the scale of experimental portion is negligible compared with the numerical counterpart. Both Equation **1** and Equation **4** converge to the numerical substructure and the RTHS error in this case is not significant even with the existence of relative large Δ and δt. This conclusion can be intuitively generalized to other types of specimens, and a good qualitative measure is the ratio between the magnitude of the generalized forces in the experimental and computational components.

Case 3: Another special case is when both substructures have identical modal characteristics i.e. damping ratios and natural frequencies. This situation is achieved by enforcing the computational model to be exactly linear proportional to experimental substructure so that $M_e = \lambda M_n, C_e = \lambda C_n, K_e = \lambda K_n$, where λ is an arbitrary constant. In this case $\omega^2 = (K_n + K_e)/(M_n + M_e) = K_e / M_e$ and the artificial damping terms in Equation **4** are cancelled out. Stability is not a concern here despite tracking error.

Case 4: The most generalized RTHS setup is when an arbitrary allocation is allowed between the mass and stiffness of the substructures. Assume $\alpha = M_e / M_n, \beta = K_e / K_n$ so that the artificial RTHS damping term in Equation **4** is:

$$M_e\omega^2 - K_e = M_e(K_n + K_e)/(M_n + M_e) - K_e = (\alpha - \beta)/(1+\alpha)K_n \qquad \text{Equation 5}$$

It is easy to observe the worst-case scenario occurs when K_n is zero which yields a singular point and $\beta \to \infty$ (i.e. infinity negative damping). In addition it is assumed $\alpha \to 0$ that provides no cancellation of the negative damping. This situation has been observed during validation experiments, and in the practices considered herein a small K_n is included to perform a successful RTHS.

Applying similar reasoning, a controller that is too aggressive can sometimes cause a phase lead i.e. $\delta t<0$ which results in artificial added damping into Equation **4**. Although this may help to stabilize the RTHS system, test accuracy will be severely compromised. Therefore a high performance tracking control strategy becomes an indispensable component of a high fidelity RTHS framework. Although most applications fall within cases 2, 3 and 4, the experimental studies considered herein focus on case 4, the most challenging case, to examine the limit of tracking controller

performance. More quantitative characterization of Δ and δt will be discussed in the following chapters, along with the proposed H_∞ control strategy to minimize these errors.

CHAPTER 3
EXPERIMENTAL SETUP

The Intelligent Infrastructure Systems Lab (IISL) houses a novel **Cyberphysical Instrument for Real-time Structural hybrid Testing (CIRST)**. This instrument was developed under NSF MRI grant number 1028668.

The instrument consists of the following cyber and physical components:

1 (Physical) Reaction Mounting System (RMS). This component supports the physical components of the simulation in a suitably stiff arrangement to perform the variety of tests needed.
2 (Cyber) Real-time Control System (RCS). This component coordinates all physical and computational actions and meets the timing constraints of a real-time hybrid test. The design strives for interoperability to facilitate implementation of any number of configurations.
3 (Physical) Sensing and Actuation System (SAS). This component includes the physical components needed to measure physical responses and apply forces during the tests.
4 (Cyber) RT-Frame2D. This open source structural analysis tool has been developed using an Embedded Matlab function to simulate the complex, nonlinear behaviors of the numerical component of the hybrid simulation in real-time.
5 (Cyber) Visualization and Control Dashboard (VCD). This component allows the user to configure each test, run offline simulations, and integrate physical and virtual sensor data with a virtualization of the entire structure for visualizing the test results.

3.1 Reaction Mounting System

This component supports the physical components of the simulation in a suitably stiff arrangement to perform the variety of tests needed. This support mechanism is reconfigurable as needed for each real-time hybrid test to be conducted. A reinforced concrete reaction is designed and constructed with a strong floor that measures 14’x10.5’x18”. Strong walls cover the floor area that is 5’x16”. Inserts and steel sleeves on a 5”x5” grid are embedded into the testing area floor and walls therefore enable multiple actuators to be flexibly placed in a three dimensional configuration.

3.2 Real-time Control System

This component coordinates all physical and computational actions to meet the timing constraints of a real-time hybrid simulation. A reconfigurable design facilitates interoperability in the computing and networking hardware. The real-time control system is implemented using the xPC framework. A high performance Speedgoat/*xPC* real-time kernel is utilized as the target PC for the proposed framework. It is configured with state-of-the-art Core i5 3.6GHz processor optimized for complex and processing intensive

computational models to execute in real-time. High-resolution, high accuracy 18-bit analog I/O boards are integrated into this digital control system that supports up to 32 differential simultaneous A/D channels and 8 D/A channels, with a minimum I/O latency of less than 5 micro-seconds for all channels. The system is intended to be reconfigurable and will allow any researcher to implement a control system, so long as it can run in real-time. The xPC system is combined with a Shore Western SC6000 analog servo-hydraulic control system to enable high precision motion control of hydraulic actuators.

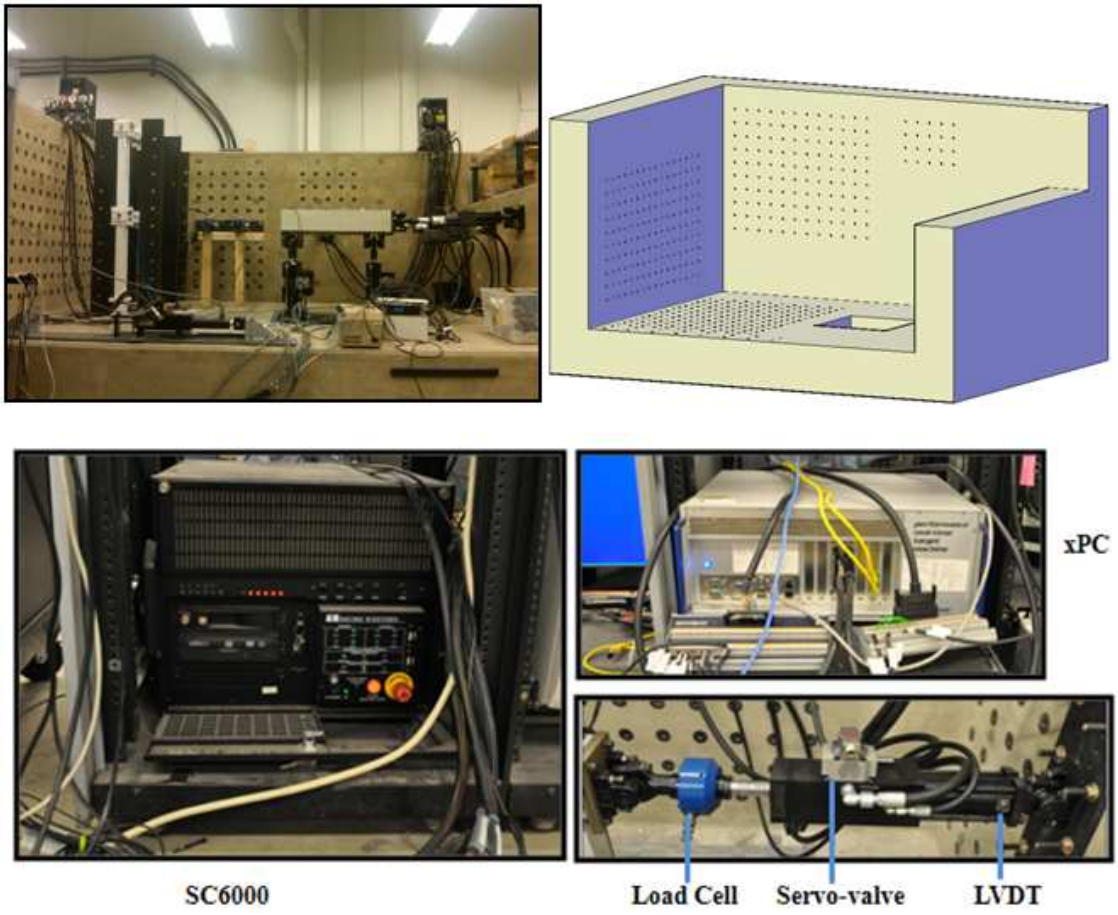

Figure 2: CIRST System Development

3.3 Sensing and Actuation (SAS) System

The SAS measures the responses of the physical components and to apply appropriate control actions during each test. Actuation is performed with up to six low-friction, double-ended, dynamically-rated hydraulic linear actuators. Four actuators have a nominal force capacity of 2.2kip and are equipped with 10gpm servo-valves, the remaining two actuators are 1.1kip with 5gpm servo-valves. All actuators are operated at the nominal fluid pressure of 2,800psi. Each actuator is equipped with both an LVDT and

a force transducer, allowing the flexibility to be used either in displacement or force feedback control modes (or mixed mode). The maximum stroke for all actuators is 4". Sensing is achieved using various types of sensors that are needed both to measure structural responses from the physical elements of the structure and to control actuation devices (force, displacement, pressure). Accelerometers, displacement sensors, strain gages, and load cells are all available for use within the CIRST for real-time hybrid simulations as needed.

3.4 RT-Frame2D

The computational tool developed in the IISL that is used to perform nonlinear dynamic analysis of steel buildings under real-time execution has been named RT-Frame2D.

Mass is modeled with a concentrated-lumped scheme by evenly distributing the mass contribution carried by horizontal/beam elements at corresponding global translational degrees of freedom (DOF). Damping effect can be represented with either a mass/stiffness proportional damping or a Rayleigh damping modeling options. Column elements are modeled as linear-elastic elements. Second order effects (P-Delta) are modeled by assuming the accumulated weight at each floor acting as constant compressive-axial forces on the corresponding column elements to calculate the geometric stiffness matrices that can be globally assembled to account for the overall P-Delta effect. Beam elements can be represented by two schemes. A moment-curvature type nonlinear beam element; which implements a hysteresis model to represent yielding locations at element ends that occur at the moment resisting beam-column connections. The hysteresis properties can be predefined depending on the element section. The yielding locations can be represented with either a spread plasticity model (SPM) or a concentrated plasticity model (CPM). Additionally, an elastic beam element with a linear/nonlinear zero-length rotational springs located at the element ends is also available. Hysteresis properties can also be predefined for each spring element. Two different material models adequate for steel structure are available for the two previous nonlinear beam models; a bilinear and tri-linear model with kinematic hardening. Panel-zone effects at column-beam connections are represented by a new model proposed by Hjelmstad and Haikal (Hjelmstad, 2006). Two models are offered: a rigid-body version and a linear version with bidirectional tension/compression and shear distortion effect. Two integration schemes are available for solving the nonlinear equation of motion and evaluate the nonlinear response; the explicit-unconditional stable Chen-Ricles (CR) algorithm (Chen, 2008) and the implicit-unconditional stable Newmark-Beta method with constant acceleration (Newmark, 1959).

The computational tool has been implemented as a MATLAB/Embedded function format. The Embedded function (Embedded MATLAB toolbox) supports efficient code generation to accelerate fixed-point algorithm execution for embedded systems. Additionally, MATLAB/Simulink is used to integrate the computational tool with the remaining RTHS components so a unique platform can be generated for real-time execution. Finally, the MATLAB/xPC Target is used to generate and compile a C-source

code from the Simulink model (host PC) that can be downloaded into a target real-time kernel (target PC) for execution.

3.5 Vizualization and Control Dashboard

Researchers using the CIRST will benefit from being able to configure each test using the VCD and to perform off-line simulations. The VCD is being developed as needed to integrate physical and virtual sensor data with a virtualization of the entire structure for visualizing the test results.

3.6 Frame Test Specimen

A steel MRF specimen is designed and erected in the IISL at Purdue University. The specimen was designed to perform acceptance testing and will be available for future testing needs as well. The specimen is modular, consisting of sets of horizontal beams, vertical columns and joint block panel zone elements. Each member is replaceable and can be easily re-assembled if any structural damage or plasticity occurs. Base supports are designed as pin-connections to reduce the moment gradient and avoid the formation of plastic hinges at column bases during experimentation. All parts are connected through the use of anti-lock high-strength steel bolts. S3x5.7 commercial section is used for columns while beams are welded from 2x1/8" web and 1-1/2x1/4" flanges steel bars thus assures strong-column weak-beam configuration. Core regions of panel zones are designed with steel plates of 4x3" with a thickness of 0.75". Columns are designed to be 21" height for each story and beams span are 25". The final assembly defines a height to width aspect ratio of H/W=1.75 which preserves realistic dynamic properties of similar large scale building frame structures, and allows structural yielding in a controlled manner within the force and stroke range of the hydraulic loading actuators. *Figure **3*** shows a picture of the complete MRF test specimen.

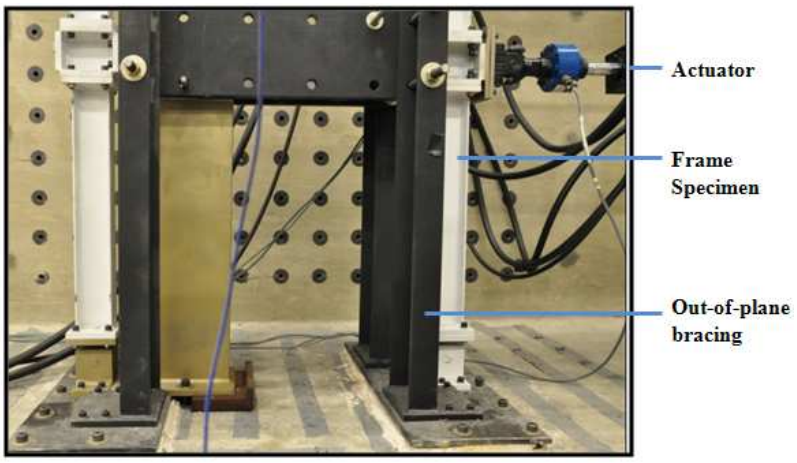

Figure 3: Frame Test Specimen

CHAPTER 4
DESIGN OF AN H_∞ TRACKING CONTROLLER

In chapter 2 we demonstrated that significant systematic experimental errors may occur in a RTHS implementation when there is de-synchronization between the computational model and the physical substructure. To achieve a high performance control, dynamic modeling techniques need to be enhanced to characterize Δ and δt over a broad frequency range. A high precision tracking control methodology is needed to accommodate the actuator dynamics and thus improve RTHS stability and accuracy.

4.1 H_∞ Controller Formulation

Here an H_∞ strategy [(Glover, 1989), (Zhou, 1998), (Matlab, 2011a)] is adopted and modified to control the motion of hydraulic actuator(s). A block diagram of the proposed controller is depicted in *Figure* ***4***. Given a dynamic plant *G(s)* that contains the overall dynamics of the inner-loop servo-hydraulic control and actuation system, the design objective is to acquire a stabilizing outer-loop controller *H(s)* which facilitates the best tracking between a desired trajectory x_d calculated from the computational model and the measured response x_m of the structural specimen. For practical reasons, a unity gain low-pass filter *F(s)* is also inserted in the feedback path. This filter is mainly needed to reduce the effect of relative large measurement noise *n*, where d_i and d_o are generalized input and output disturbances, respectively. System output sensitivity *S* and complementary sensitivity *T* are defined for a standard H_∞ control system, along with the system output expressed as

$$S = (I + GH)^{-1}, T = I - S = GH(I + GH)^{-1} \qquad \text{Equation 6}$$
$$x_m = T(x_d - n) + SGd_i + Sd_o$$

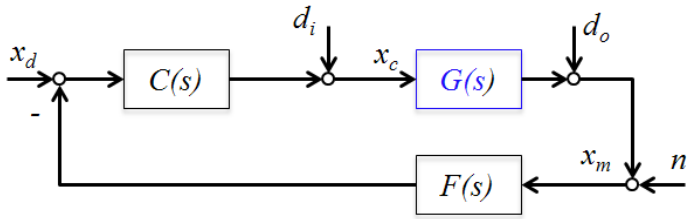

Figure 4: Formulation of Proposed Controller Implementation

It is clear from Equation **6** that one way to achieve high performance tracking and strong disturbance rejection is to choose *T* close to unity and *S* to zero. Both goals can be achieved through shaping a large open loop gain *G(s)H(s)* within the performance frequency range. Herein the loop gain is defined as the maximum singular value of a generalized multi-input, multi-output (MIMO) system that is equivalent to the magnitude of the transfer function in the special case of a single-input, single-output (SISO) system. A controller with unrealistic large loop gain is likely to yield instabilities due to

unmodeled dynamics in the physical systems. The loop gain at higher frequencies needs to be kept small to guarantee robust stability and accommodate system uncertainties. Depending on the physical plant dynamics and uncertainty level, the proposed H_∞ design philosophy is summarized as a trade-off between large loop gain for tracking performance and small loop gain for robustness.

Given the plant *G(s)*, 1st step of the H_∞ loop shaping controller design procedure is to calculate a pre-compensator *W(s)* such that the target loop shape can be represented in state space as $G_d(s) = G(s)W(s) \equiv \{A_G, B_G, C_G, D_G\}$. A stabilizing controller is then synthesized by solving the H_∞ optimization problem for tolerance level γ:

$$\left\| \begin{bmatrix} K(I - G_d K)^{-1} \tilde{M}^{-1} \\ (I - G_d K)^{-1} \tilde{M}^{-1} \end{bmatrix} \right\|_\infty \leq \gamma \qquad \text{Equation 7}$$

A particular controller is constructed that has the state space form:

$$K(s) \equiv \{A^c + \gamma^2 W_1^{*-1} Z C_G^* (C_G + D_G N), \gamma^2 W_1^{*-1} Z C_G^*, B_G^* X, -D_G^*\} \qquad \text{Equation 8}$$

where $(^*)$ denotes the complex conjugate transpose of a matrix. Two generalized algebraic Riccati equations are solved to obtain *X* and *Z* respectively:

$$\begin{aligned} &(A_G - B_G P^{-1} D_G^* C_G)^* X + X(A_G - B_G P^{-1} D_G^* C_G) - X B_G P^{-1} B_G^* X + C_G^* (I - D_G^* P^{-1} D_G^*) C_G^* = 0 \\ &(A_G - B_G D_G^* R^{-1} C_G) Z + Z(A_G - B_G D_G^* R^{-1} C_G)^* - Z C_G^* R^{-1} C_G Z + B_G (I - D_G^* R^{-1} D_G) B_G^* = 0 \end{aligned} \qquad \text{Equation 9}$$

Intermediate terms are defined and calculated as:

$$\begin{aligned} &P = I + D_G^* D_G, R = I + D_G D_G^*, U = -(Z C_G^* + B_G D_G^*) R^{-1}, N = -P^{-1}(D_G^* C_G + B_G^* X), \\ &\tilde{M} = R^{-1/2} + R^{-1/2} C_G (SI - A_G - U C_G)^{-1} U, A^c = A_G + B_G N, W_1 = I + (XZ - \gamma^2 I) \end{aligned} \qquad \text{Equation 10}$$

The final feedback controller is then constructed by combining the H_∞ controller with the shaping function such that *H(s)=W(s)K(s)*.

4.2 Controller Design

The target loop shape $G_d(s)$ for this specific validation experiment is selected as:

$$G_d(s) = \frac{2.39e5}{s^2 + 628.32s + 3.95e3} \qquad \text{Equation 11}$$

The design goal is to shape the open loop gain to match $G_d(s)$ within the tolerance level γ. T and S are calculated as well and are shown in *Figure* ***5***. In the low frequency range, S is very small to guarantee a small tracking error. At the other end, T is small in the high frequency range for increased robustness where modeling error is large.

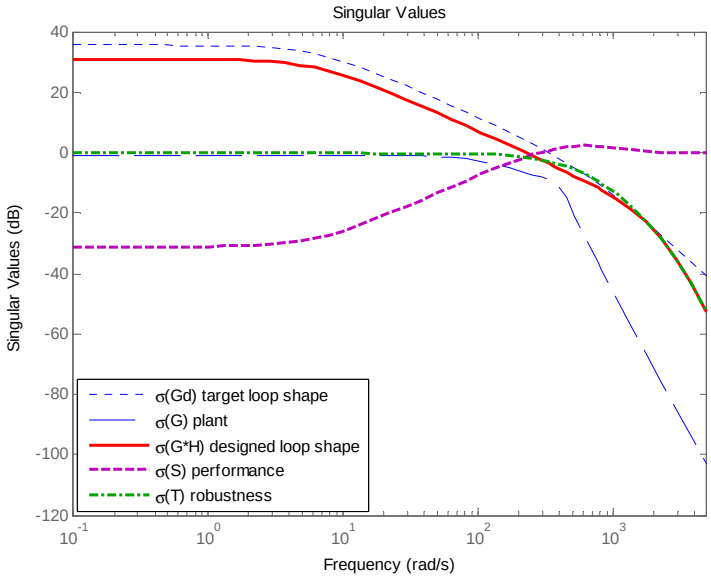

Figure 5: Controller Design

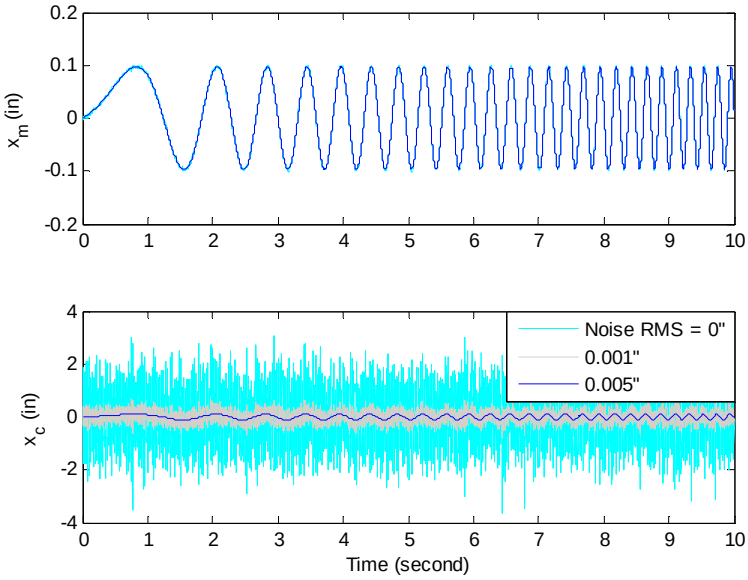

Figure 6: Effect of Measurement Noise on Command Signal

For practical implementation, an important issue is related to the measurement noise *n*. Noise rejection in this design methodology is conflicted with the tracking perform requirement, which is clear in Equation **6**. High loop gain will enable noise being passed through, and will hinder performance in the frequency bandwidth. The relatively large actuator LVDT feedback noise present in this study could significantly affect the tracking performance without proper consideration. Numerical simulations of the system are performed to examine the effects of this noise on the RTHS control command signal. Using the experimentally identified plant model, a 0-5Hz chirp signal at an amplitude of 0.1" is used as the desired trajectory. Three different noise levels are considered with the root mean square (RMS) values of 0", 0.001" and 0.005", respectively. Notice from the results shown in *Figure **6*** that even a small amount of noise can have dramatic influence on the performance of the closed-loop control system. The controller may magnify the broadband noise significantly and contaminate the calculated command trajectory x_c. The measured trajectory x_m does not seem to be affected much because the plant model acts as a physical low-pass filter to reduce high frequency effects. This implementation is very risky in practical design because unmodeled dynamics can be excited which is likely to induce instabilities. Another design goal to keep the controller less aggressive is to avoid input saturation. Having a large loop gain outside of the bandwidth of the plant i.e. $GH>>I$ and $G<<I$ is likely to cause actuator saturation.

A unity gain 2nd order Butterworth, low-pass filter *F(s)* with a cutoff frequency of *50Hz* is applied in our design for noise filtering. This choice of filter is made for two primary purposes: 1) to reduce the effect of measurement noise; and 2) to further enhance phase tracking in addition to the primary controller *H(s)*. *Figure **7*** provides a plot of the transfer function of the plant used in this study from command to measured displacement, and comparisons of outer-loop control system with and without *F(s)*. Identified plant model is also compared.

$$G(s) = \frac{4.52e9}{s^4 + 577s^3 + 2.68e5s^2 + 6.28e7s + 4.93e9}$$ Equation 12

Note that although it is possible to improve tracking performance by designing a more aggressive primary controller, a moderate target loop shape is essential to balance the requirement of control system robust stability. Clearly this filter, *F(s)*, is beneficial to achieve nearly perfect phase tracking between 0-25Hz, but its presence also introduces magnitude amplification due to the additional system poles. Despite the outstanding behavior of the designed controller demonstrated subsequently in chapter 5 and 6, there could be a negative influence of these poles on the overall RTHS dynamics. For each specific experiment, the designer must evaluate numerous factors such as the desired performance bandwidth, physical system uncertainty bound and measurement noise level to design an effective optimal controller.

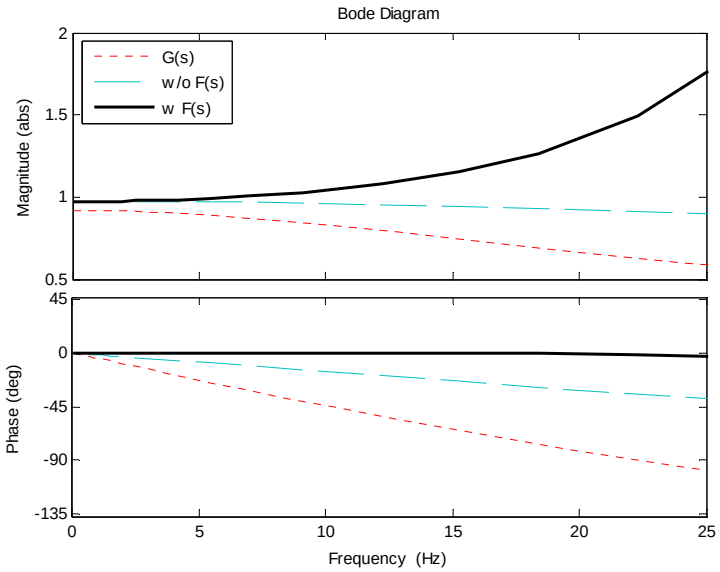

Figure 7: Transfer Functions of Displacement Tracking

CHAPTER 5
ANALYSIS AND SIMULATION

A generalized analysis procedure from a dynamical system perspective is proposed and applied in this chapter to evaluate the various RTHS components and complex interactions. The study employs the values from the experimental components discussed in chapter 3. Several control strategies are evaluated including the proposed H_∞ controller, and a series of comprehensive RTHS systems are thus constructed and compared against reference structural systems. The procedure is demonstrated to be useful to predict the RTHS stability limit and performance accuracy before a physical test is conducted.

5.1 Test Matrix Construction

Selection of the numerical substructure parameters is based on the worst case scenario (Case 4) discussed in chapter 2. Experimental specimen properties are first identified and listed in *Table **1***. Note that the physical damping C_e is challenging to identify accurately when the hydraulic actuator is attached. The influence of C_e on RTHS accuracy is elaborated on more in chapter 6. A small amount of numerical stiffness K_n is assumed in the computational model to avoid the mathematical singularity in this formulation.

A series of systems are constructed by assuming different values of the natural frequency ω of the reference structure (Equation **1**). The total mass is determined for each chosen ω and the total damping ratio is assumed to be *2%* in each reference system. The numerical mass and damping are thus obtained by subtracting the experimental parts from the reference structure. This imbalance of mass and stiffness configuration represents the largest contribution to the RTHS system artificial negative damping (Equation **5**), e.g. when ω*=1Hz,* α*=3.9e-4* that is negligible but the stiffness is exactly the opposite with β*=100*.

	Experimental	Numerical	Reference
Mass (lb-s^2/in)	M_e=8.55e-2	$M_n=M_t-M_e$	$M_t= K_t/\omega^2$
Stiffness (lb/in)	K_e=8.6e3	$K_n=0.01*K_e$	$K_t= K_e+K_n$
Damping (lb-s/in)	C_e=5.42	$C_n=C_t-C_e$	$C_t=2*0.02*(M_t*K_t)^{1/2}$

Table 1: Test Matrix Structure Parameters

One quick way to estimate the maximum allowable system delay, once the test setup is determined, is by calculating damping term in Equation **4**. If we assume perfect amplitude tracking $\Delta=1$, $\delta t_{\max} \le C_t/(K_e - M_e\omega^2)$ is a useful index to evaluate the RTHS system stability margin. Δ can be obtained more accurately using the transfer function magnitude between desired and measured displacements, once a tracking controller is

selected. *Figure **8*** shows this tolerable delay limit for the chosen test matrix in this study and demonstrates the technical challenges. Dramatic challenges arise as the frequency ω increases because 1) the physical actuator has to track a faster signal; 2) the physical substructure that carries the most experimental error comprises a larger portion as the numerical mass is reduced. Notice that about 1/3 millisecond (ms) delay drives the RTHS system to instability when ω increases. For the actuators use in this study, the inner-loop servo-actuator delay is about 12-13ms within the bandwidth of interest. Thus, without a motion control system, a stable RTHS cannot be achieved even at a very low frequency of ω*=1Hz*. This conclusion is validated and shown experimentally later.

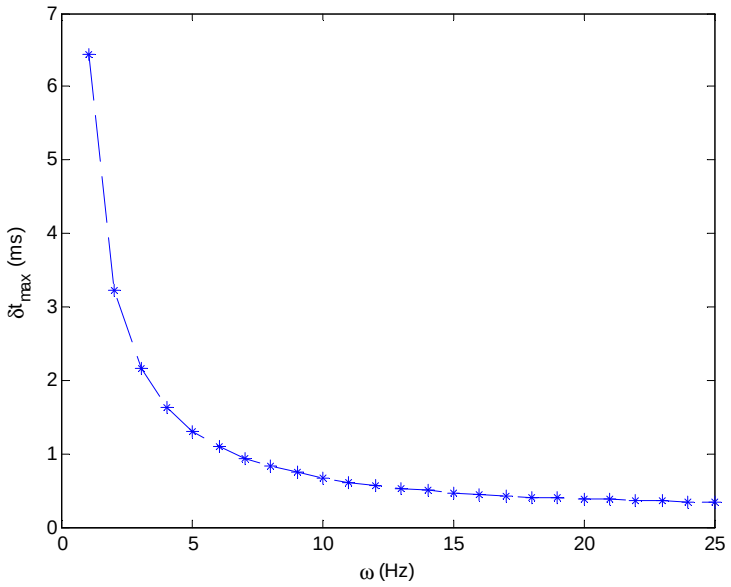

Figure 8: Maximum Allowable Delay

5.2 System Error Analysis

The dynamics of the closed-loop RTHS systems are analyzed before conducting any physical experiments. A reference structure is used to examine the system error. In addition to the proposed H_∞ strategy, both a model based (Carrion, 2007) and an inverse compensation strategy (Chen, 2007) are implemented and evaluated. Optimal controller parameters are chosen as α_{mb}*=17* and α_{inv}*=15*, respectively, which are determined from both simulation and tracking experiments using a pre-defined 0-10 Hz chirp displacement trajectory. Each of the RTHS system transfer functions are compared in *Figure **9*** when ω*=8Hz*. It is clear that the proposed H_∞ strategy does match the reference system dynamics very well, especially near the system's fundamental frequency. The other RTHS systems considered appear to yield significant natural frequency shifts and damping reductions. Analysis shows that a slightly increased frequency ω*=9Hz* will cause system instabilities. One drawback of the proposed strategy is that it introduces a 2nd mode at around 37Hz due to the aggressive low-pass filter in the H_∞ control design.

Although we need to be aware of it, this mode is beyond the bandwidth of typical earthquake engineering applications. We should also aim to ensure that the electronic noise in the measurements is low.

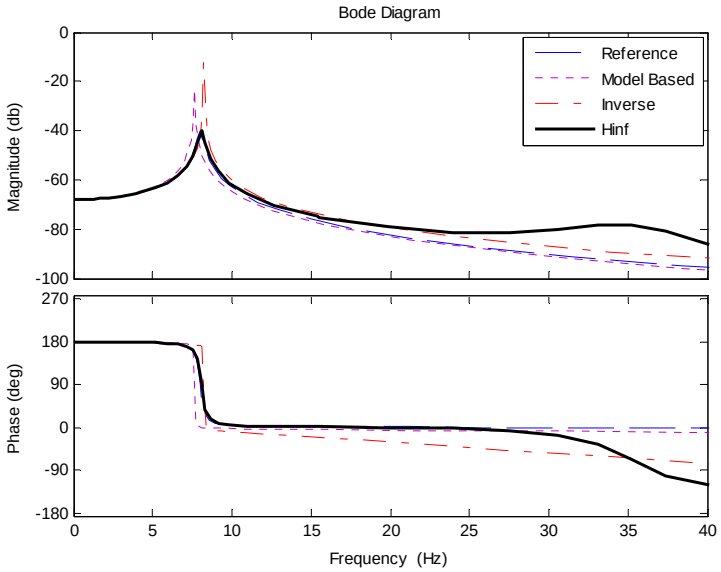

Figure 9: Transfer Functions of Overall RTHS Systems

In these lightly damped systems the essential dynamics can be characterized by the maximum gain, i.e. transfer function magnitude peak (M_{RTHS}), and its associated frequency (ω_{RTHS}). The normalized maximum system gain error is thus defined as the Euclidean norm of the distance between the RTHS and the reference system maximum gains (M_{REF}).

$$E_{SS} = \sqrt{\left(M_{RTHT} / M_{REF} - 1\right)^2 + \left(\omega_{RTHT} / \omega - 1\right)^2}$$

This index is useful to capture both the shift in the system frequency and the error in the magnitude. The normalized error for each of the system is plotted against the resonant frequency in *Figure* ***10***. Larger errors indicate that the RTHS system is approaching unstable behavior.

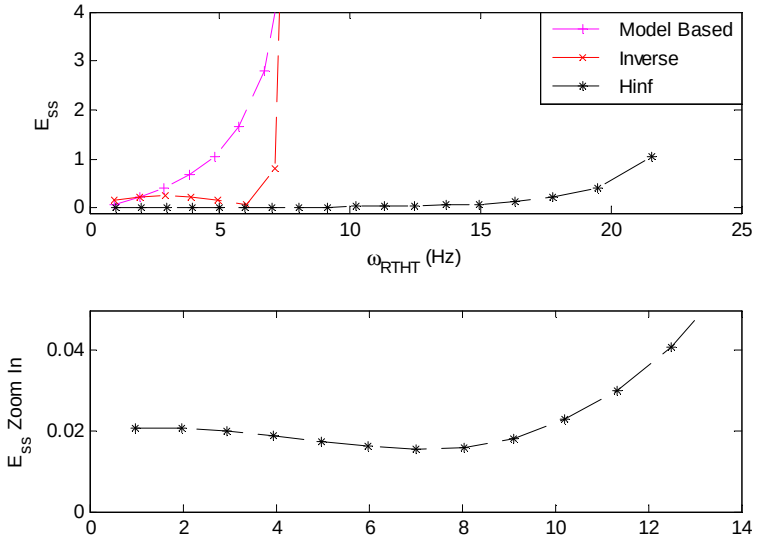

Figure 10: Normalized RTHS System Error

CHAPTER 6
EXPERIMENTAL RESULTS AND ROBUSTNESS

The procedure discussed in chapter 5 is repeated with the single story frame experiment. The frame is subjected to the NS component of the 1940 El-Centro earthquake. The intensity is varied from 0.02 to 3 taking into account the actuator force capacity and the stroke. All tests are conducted at a sampling rate of 1024Hz.

6.1 Performance Evaluation

The RMS values of the normalized RTHS error (E_{RTHT}) and the actuator tracking error ($E_{Tracking}$) are calculated and shown in *Figure **11*** where errors are evaluated at each time step i of the whole response time histories. Note that only the feed-forward portion of the model based compensator is implemented and assessed for this test matrix. Linear inverse compensator is herein evaluated since the frequency domain analysis tools are not applicable when the adaptive mechanism is included.

$$E_{RTHS} = \sqrt{\frac{\frac{1}{N}\sum_{i=1}^{N}(x_{ref,i} - x_{d,i})^2}{\frac{1}{N}\sum_{i=1}^{N}(x_{ref,i})^2}} \times 100\% \text{ , } E_{Tracking} \sqrt{\frac{\frac{1}{N}\sum_{i=1}^{N}(x_{d,i} - x_{m,i})^2}{\frac{1}{N}\sum_{i=1}^{N}(x_{d,i})^2}} \times 100\%$$

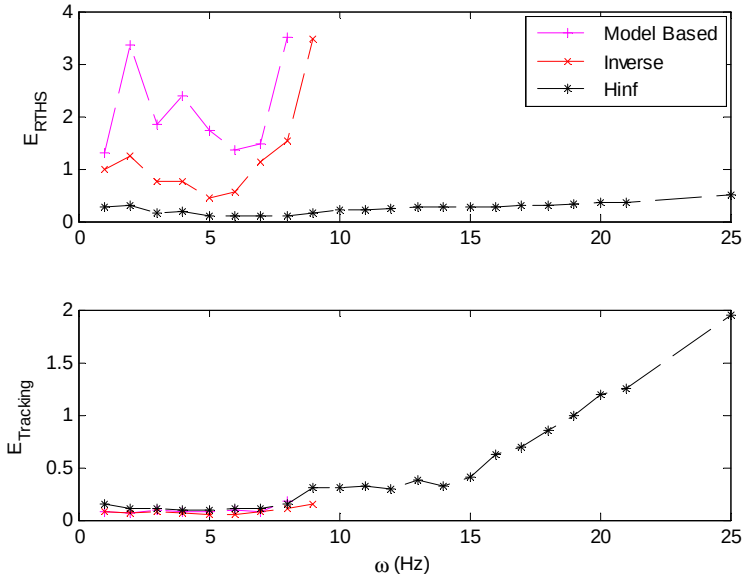

Figure 11: Normalized RTHS and Tracking Error

Several important observations are made:

1) The inner-loop PID control alone is not adequate to run a stable RTHS test even at the low natural frequency of ω*=1Hz*. This observation demonstrates that the selected experimental setup is indeed quite challenging and therefore requires a high quality motion controller.
2) The proposed H_∞ controller can significantly extend the RTHS stability limit to ω*=25Hz*.
3) In general, the proposed H_∞ controller achieves the smallest RTHS error. This conclusion is clear from both the frequency domain analysis (*Figure **10***) and time domain experimental results (*Figure **11***).
4) Strong correlations are observed between the analysis and experimental results. Specifically the stability limit of 8-9Hz is successfully predicted for both the model based and the inverse controllers. In terms of accuracy, the inverse controller can achieve the smallest error at ω*=6Hz* as indicated by analysis. The relative large error of model based controller and its inconsistency with analysis results is related to errors in the system identification process. This discrepancy is addressed in the next section.

The results from this study increase the creditability of performing offline simulation to investigate more complicated RTHS systems. Important issues can be investigated that may be difficult to study experimentally, such as parameter sensitivity, characterization of system uncertainty bounds etc. Controller stability and performance limits can be enhanced when more physical system information is available.

*Figure **12*** provides time histories of the RTHS responses using the H_∞ controller. They are compared with the time histories of the reference structural responses at ω*=1* (12-a), *5* (12-b) and *15Hz* (12-c), respectively. Good comparisons are observed in all cases, demonstrating the effectiveness of the proposed control strategy. The comparison of responses with ω*=5Hz* shows better match than at 1Hz, which appears to be counterintuitive. The proposed system analysis procedure is able to predict this successfully as shown in *Figure **10***.

Additional challenges exist when the earthquake magnitude is small such as at the end of the earthquake. The comparison is not as good due to the presence of a relative large noise to signal ratio. For instance, focusing on the region between 40-43 seconds (lower right subplot in each), high frequency oscillations occur because the 2nd mode of the H_∞ RTHS system is excited by the measurement noise. This effect is more significant at higher frequencies such as when ω*=15Hz* that is approaching the 2nd mode of RTHS system. This type of oscillation is a common observation in RTHS community and is reported by other researchers (Bonnet, 2007). Representative time domain comparisons are also made for the various control strategies in *Figure **13*** when experiments are conducted at ω*=5Hz*. The results demonstrate the superior performance of the proposed H_∞ controller.

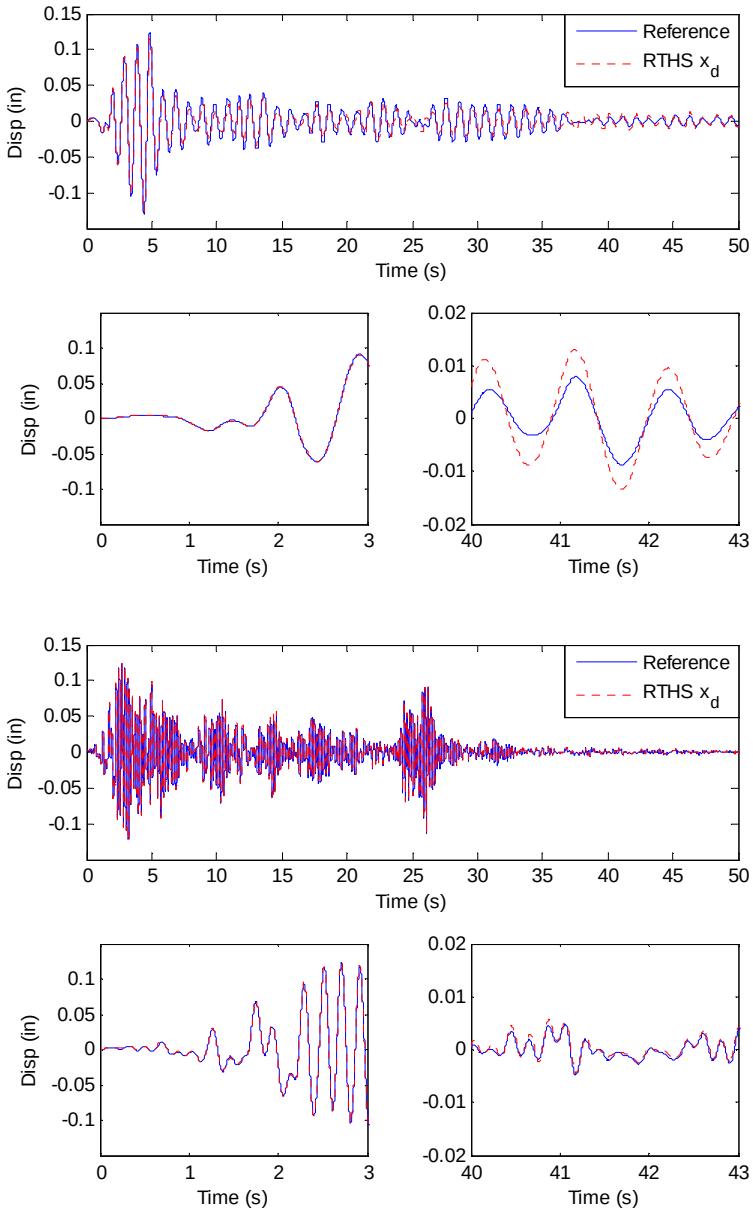
Reference
RTHS x_d
Disp (in)
Time (s)
0.15
0.1
0.05
0
-0.05
-0.1
0
5
10
15
20
25
30
35
40
45
50
0.02
0.01
-0.01
-0.02
1
2
3
41
42
43

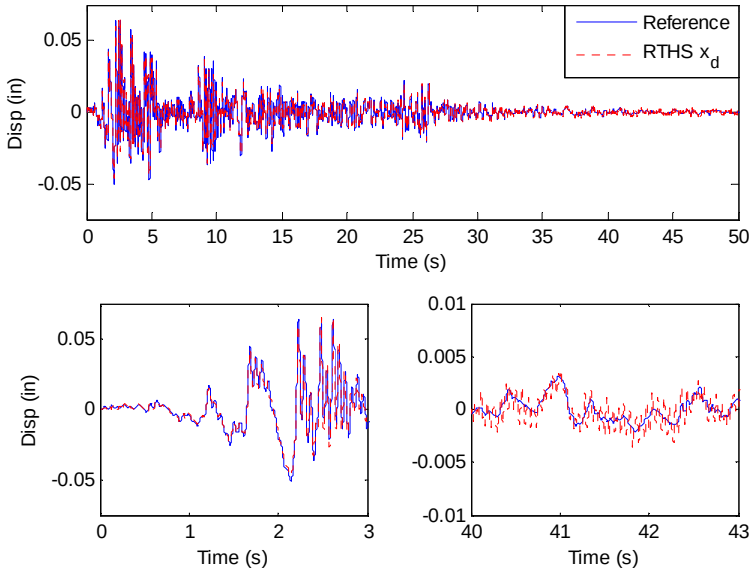

Figure 12: (a, b, c) H∞ Controller RTHS Error Assessment

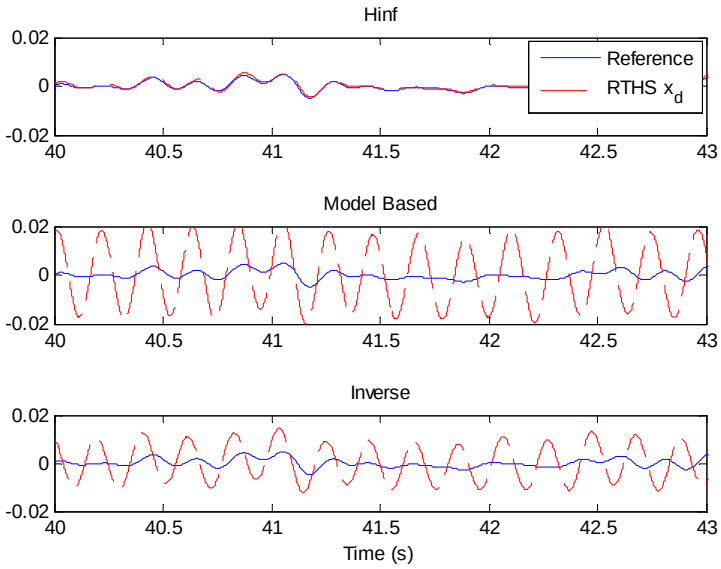

Figure 13: RTHS Error Using Various Controllers

Another interesting observation considers the apparent contradiction between RTHS error and tracking error in *Figure* ***11***. Although the H_∞ controller shows the smallest RTHS error in general, the RMS tracking error is relatively large due to the presence of a 2nd mode of the closed-loop system. The experimental tracking error time histories at ω_t*=5Hz* are shown in *Figure* ***14***. It is clear that significant RMS error is contributed by this local high frequency oscillation. Although this effect is not ideal, the good match shown in *Figure* ***12*** demonstrates that the global dynamics are maximally

preserved using the proposed H_∞ controller. Improved hardware with a small noise level is essential for high quality RTHS implementation. One way to minimize the effects of noise is to use larger input earthquake intensity. This observation also leads to the conclusion that the tracking error RMS value alone may not be sufficient to fully characterize a controller's performance in terms of RTHS accuracy.

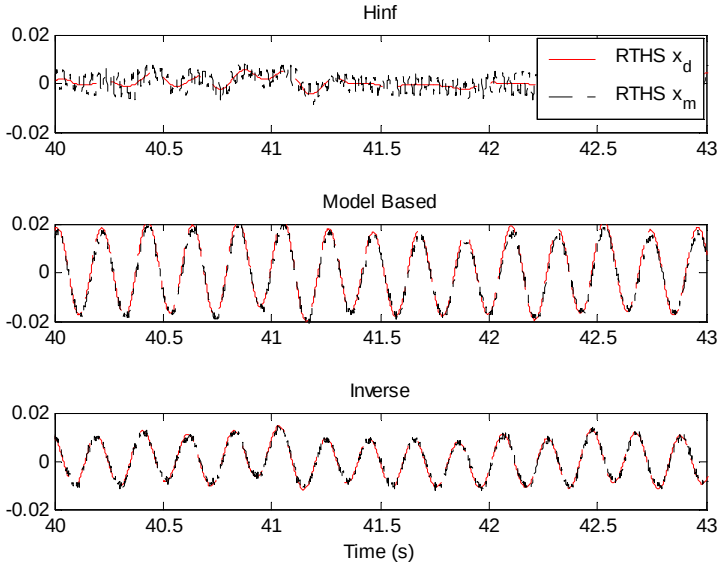

Figure 14: Actuator Tracking Error Using Various Controllers

6.2 Controller Robustness Evaluation

Much of the attention so far has been put on the nominal tracking performance of the motion controller. Although analysis based on linear time invariant systems are good enough to capture the essential dynamics, parameter uncertainty and unmodeled dynamics are inevitable in the physical system. A relevant example in the structural engineering community is the structural nonlinearity that can arise during the test of a frame specimen. Also all actuator mechanical parts have their own nonlinearities that are not considered in the control design. Having a robust controller is highly desirable for the ultimate RTHS goal of testing complex systems that may not have a reliable model. High quality parametric identification in these cases may be very challenging to perform, or perhaps impossible.

Here we evaluate the robustness of the controller design by introducing uncertainty in a controlled manner. The inner-loop controller P gain is changed from the nominal value of 3.0 to both 2.5 and 3.5. Then the tests at ω=*6Hz* are repeated without identification or redesign (i.e. the original controller is applied). The various actuator control strategies are tested on the new systems for robustness and the results are shown

in *Figure* ***15***. Clearly the H_∞ controller has quite consistent performance, and the feed-forward controllers are not as effective, especially when the P gain is reduced.

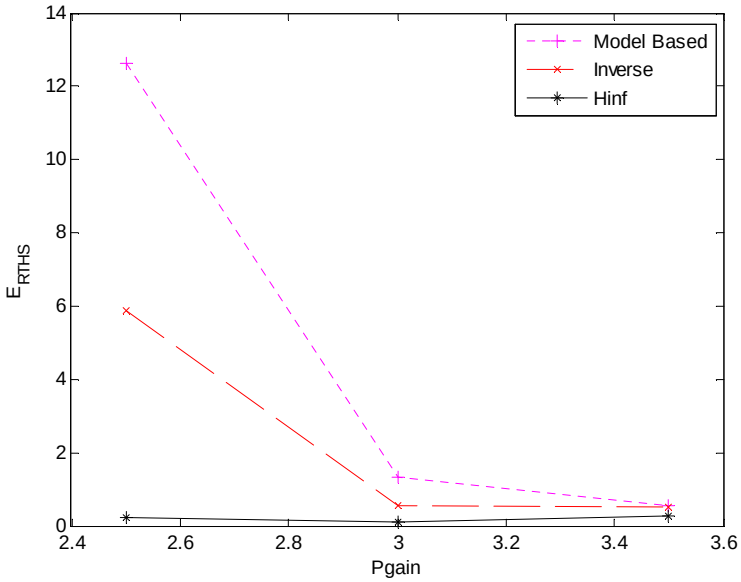

Figure 15: Controller Robustness Assessment

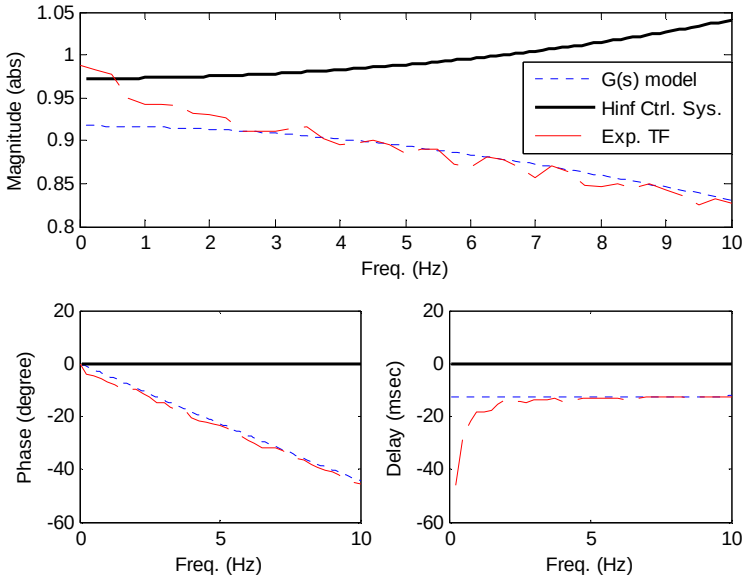

Figure 16: Identification Error and Control Design

Another demonstration for the H_∞ controller robustness is to consider the identification error. A relative sharp magnitude slope change is observed at a low frequency in the plant experimental transfer function (*Figure* ***16***) from the actuator command to the measured displacement. The assumed form of the plant (Equation **12**) in this study has four poles and none zeros, and cannot capture this behavior. The plant

model is curve-fitted through a least square optimization algorithm so that local behavior like this is not accurately reflected. The DC gain of the plant model is therefore less than unity which may partially explain why the performance of model based strategy is not as good as one might expect. Despite this modeling imperfection and identification error, the proposed H_∞ controller behaves very well. The robustness feature herein reduces the dependence of controller performance on the prior identification accuracy.

6.3 Experimental Error Correction

One of the key reasons one might choose to perform RTHS is to preserve the rate dependent characteristics of experimental substructure. Although small in scale, the structure used in this study represents a typical moment resistant frame that is commonly used in civil engineering practice. The frame carries significant stiffness but very small mass and damping, which would normally be ignored, for instance in slow speed PsD testing. This assumption is justifiable when ω is small but will cause error at higher ω because the velocity and acceleration terms play a more significant role. The test matrix selected herein provides a good demonstration to justify the need for performing these tests in real-time and to preserve these higher order dynamics.

The light dashed curves in *Figure **17*** correspond to the results obtained when physical M_e and C_e are not considered. The dark solid curves are obtained with a correction made to subtract these small but significant values from numerical substructure. Therefore the solids curves maintain the correct amount of total structure properties (the summation of numerical and experimental substructures) compared with the reference structure. The H_∞ controller can achieve significant reduced RTHS errors when making this correction, but the other two controllers appear oppositely to yield even larger errors. Note that this may explain why the approach of adding significant numerical damping often works during a RTHS to balance the negative damping caused by inappropriately compensated actuator delay. This study shows furthermore the importance of having a high precision motion tracking controller to achieve good RTHS accuracy. The damping in a continuous frame structure may be quite complicated, or even nonlinear, especially when the hydraulic actuator is connected and interacts with the frame. Although it is possible to further reduce RTHS error by adjusting damping value for each individual test, the optimal value of C_e*=5.42 lb-s/in* is assumed for all tests herein to keep the consistency. This value is equivalent to 10% proportional damping of the physical MRF substructure, but still quite small compared to the assumed reference structure total damping. It is intended to be an initial simplified procedure to consider the actuator contribution/interaction **(Dyke, 1995)** into the RTHS system. Further understanding is needed to model the dynamic coupling and interaction between actuator and specimen. Although the proposed H_∞ strategy can already achieve excellent displacement tracking performance, a more refined force correction mechanism may be another important RTHS component to further enhance the test accuracy.

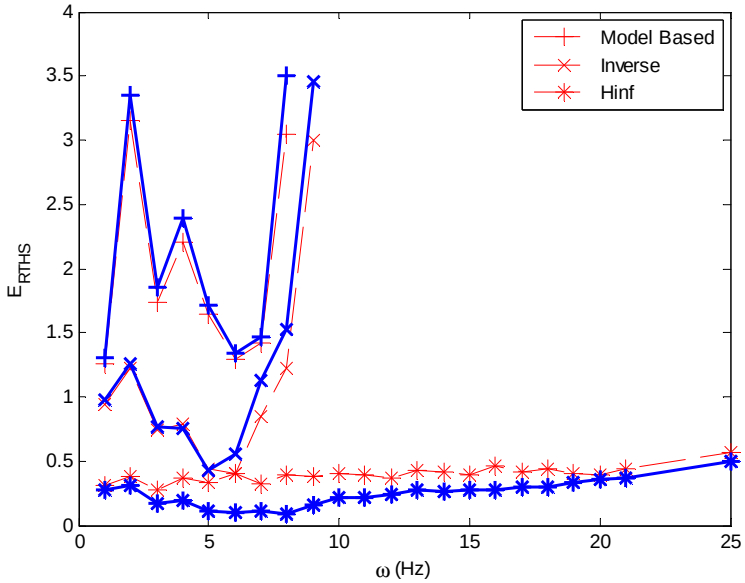

Figure 17: Effect of Experimental Mass and Damping

CHAPTER 7
CONCLUSIONS

A new servo-hydraulic actuator motion control strategy suitable for RTHS is proposed. The proposed H_∞ strategy is characterized not only by superb performance in terms of stability and accuracy, but also by strong robustness in terms of physical system uncertainties. It is demonstrated both analytically and experimentally that the significance of RTHS error depends not only on the actuator motion tracking error, but also heavily on the partitioning of the structure between numerical and experimental components. The worst-case scenario is analyzed and extensively validated experimentally. The proposed physical MRF specimen and assumption of computational model may be ideal as a benchmark problem to evaluate tracking controller performance limitations. Under this configuration, experimental mass and damping of a typical MRF contribute considerably to the hybrid testing accuracy. This emphasizes the importance of real-time testing to preserve higher order dynamics even for conventional structural members, not to mention more advanced vibration mitigation devices that are highly rate dependent.

REFERENCES

Blakeborough, A., Williams, M. S., Darby A. P. and Williams, D. M. “The Development of Real-time Substructure Testing.” *Phil. Trans. Royal Society* 359 (2001): 1869-1891.

Bonnet, P. A., Lim, C. N., William, M. S., Blakeborough, A., Neild, S. A., Stoten, D. P. and Taylor, C. A. “Real-Time Hybrid Experiments with Newmark Integration, MCSmd Outer-Loop Control and Multi-Tasking Strategies.” Earthquake Engineering and Structural Dynamics 36, no. 1 (2007): 119-141.

Carrion, J. and Spencer, B. “Model-based Strategies for Real-time Hybrid Testing.” Newmark Structural Engineering Laboratory Report Series, Urbana, IL: University of Illinois at Urbana-Champaign, 2007.

Chen, C. and Ricles, J. M. "Development of Direct Integration Algorithms for Structural Dynamics using Discrete Control Theory." Journal of Engineering Mechanics 134, no. 8 (2008): 676-683.

Chen, C. and Ricles, J. M. “Tracking Error-based Servohydraulic Actuator Adaptive Compensation for Real-time Hybrid Simulation.” Journal of Structural Engineering 136, no. 4 (2010): 432-440.

Chen, C. Development and Numerical Simulation of Hybrid Effective Force Testing Method. Ph.D. dissertation, Bethlehem, PA.: Dept. of Civil and Environmental Engineering, Lehigh Univ., 2007.

Darby, A. P., Williams, M. S. and Blakeborough, A. “Stability and Delay Compensation for Real-Time Substructure Testing.” Journal of Engineering Mechanics 128, no. 12 (2002): 1276-1284.

Dyke, S. J., Spencer, B. F., Quast, P. and Sain, M. K. “The Role of Control-Structure Interaction in Protective System Design.” ASCE Journal of Engineering Mechanics 121, no. 2 (1995): 322-338.

Glover, K. and McFarlane, D. “Robust Stabilization of Normalized Coprime Factor Plant Descriptions with H∞-bounded Uncertainty.” IEEE Transactions on Automatic Control 34, no. 8 (1989): 821-830.

Hjelmstad, K. D. and Haikal, G. "Analysis of Steel Moment Frames with Deformable Panel Zones." Steel Structures, 2006: 129-140.

Horiuchi, T., Inoue, M., Konno, T. and Namita, Y. “Real-Time Hybrid Experimental System with Actuator Delay Compensation and its Application to a Piping System with

Energy Absorber." Earthquake Engineering and Structural Dynamics 28, no. 10 (1999): 1121-1141.

Lim, C. N., Neild, S. A., Stoten, D. P., Drury, D. and Taylor, C. A. "Adaptive Control Strategy for Dynamic Substructuring Tests." Journal of Engineering Mechanics 113, no. 8 (2007): 864-873.

Magonette, G. "Development and Application of Large-scale Continuous Pseudodynamic Testing Techniques." Phil. Trans. Royal Society 359 (2001): 1771-1799.

Matlab. http://www.mathworks.com. 2011a.

Merritt, H. E. Hydraulic Control Systems. New York: Wiley, 1967.

Nakashima, M. and Masaoka, N. "Real-Time Online Test for MDOF Systems." Earthquake Engineering and Structural Dynamics 28, no. 4 (1999): 393-420.

Newmark, N. M. "A method of computation for structural dynamics." Journal of Engineering Mechanics Division 85 (1959): 67–94.

Pillips, B. M. and Spencer, B. F. "Model-Based Servo-Hydraulic Control for Real-Time Hybrid Simulation." Newmark Structural Engineering Laboratory Report Series, Urbana, IL: University of Illinois at Urbana-Champaign, 2011.

Reinhorn, A., Sivaselvan, M., Liang, Z. and Shao, X. "Real-time Dynamic Hybrid Testing of Structural Systems." 13th World Conference on Earthquake Engineering. Vancouver, B.C., Canada, 2004. 1644.

Shing, P., Wei, Z., Jung R. and Stauffer, E. "NEES Fast Hybrid Test System at The University of Colorado." 13th World Conference on Earthquake Engineering. Vancouver, B.C., Canada, 2004. 3497.

Wu, B., Wang, Q., Shing, P. B. and Ou, J. "Equivalent Force Control Method for Generalized Real-time Substructure Testing." Earthquake Engineering and Structural Dynamics 36 (2007): 1127-1149.

Yao, B., Bu, F. and Chiu, G. C. T. "Nonlinear Adaptive Robust Control of Electro-hydraulic Systems Driven by Double-rod Actuators." International Journal of Control 74, no. 8 (2001): 761-775.

Zhou, K. and Doyle, J. Essentials of Robust Control. New Jersey: Prentice Hall, 1998.